ACS OMEGA

http://pubs.acs.org/journal/acsodf

Article

Synthesis of Poly(methacrylic acid)/Montmorillonite Hydrogel Nanocomposite for Efficient Adsorption of Amoxicillin and Diclofenac from Aqueous Environment: Kinetic, Isotherm, Reusability, and Thermodynamic Investigations

Suhail Ayoub Khan, Mohammad Fuzail Siddiqui, and Tabrez Alam Khan*

Cite This: *ACS Omega* 2020, 5, 2843−2855

Read Online

ACCESS | Metrics & More | Article Recommendations | Supporting Information

ABSTRACT: Herein, a simplistic redox polymerization strategy was utilized for the fabrication of a poly(methacrylic acid)/montmorillonite hydrogel nanocomposite (PMA/nMMT) and probed as a sorbent for sequestration of two pharmaceutical contaminants, viz., amoxicillin (AMX) and diclofenac (DF), from wastewater. The synthesized hydrogel nanocomposite was characterized by the Fourier transform infrared, X-ray diffraction, X-ray photoelectron spectroscopy, scanning electron microscopy−energy dispersive X-ray spectroscopy, and transmission electron microscopy techniques to analyze structural characteristics and sorption interactions. The efficacy of PMA/nMMT was thoroughly investigated for the sequestration of AMX and DF from the aquatic phase with a variation in operative variables like agitation time, sorbent dosage, pH, and initial sorbate concentration. The reaction kinetics was essentially consistent with the pseudo-second-order model with rate dominated by the intraparticle diffusion model as well as the film diffusion mechanism. The Freundlich isotherm appropriated the equilibrium data over the entire range of concentration. Thermodynamic investigation explored the spontaneous and endothermic nature of the process. The most possible mechanism has been explained, which includes electrostatic interaction, hydrogen bonding, cationic exchange, and partition mechanism. Economic feasibility, better sorption capacity (152.65 for AMX and 152.86 mg/g for DF), and efficient regeneration and reusability even after four consecutive sorption−desorption cycles ascertained PMA/nMMT as a potential sorbent for AMX and DF uptake from the aqueous phase.

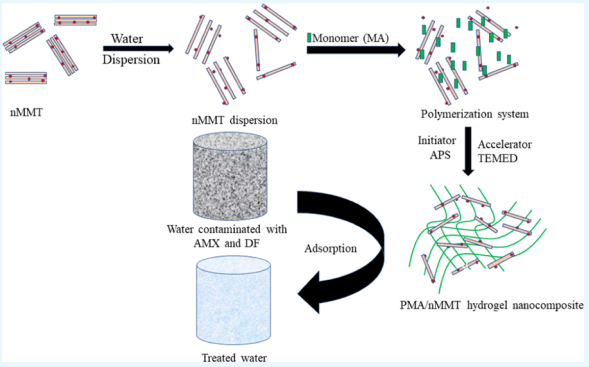

INTRODUCTION

Aqueous effluents emanating from pharmaceutical industries, hospitals, municipal areas, and body discharges[1] are generally contaminated with numerous hazardous organic pollutants, which are rarely biodegradable even at a low concentration range.[2] The release of emerging contaminants into the ecosystem has obnoxious effects on ecological species and poses a substantial threat to the human and aquatic health.[3] Among the pollutants derived from pharmaceutical industries, amoxicillin (AMX) and diclofenac (DF) were selected as probe molecules because they are extensively used and ubiquitously found in aqueous bodies.[4] Amoxicillin belongs to the group of β-lactam antibiotics with characteristic properties of treating bacterial infection, pneumonia, strep throat, and urinary tract and skin infection.[5] Diclofenac being an anti-inflammatory and nonsteroidal drug is broadly used to appease inflammation, pain caused by migraine, arthritis, gout, and some other illnesses.[6] However, they are not entirely metabolized upon consumption and approximately 10−15% of these compounds are excreted and subsequently discharged into the environment due to incompetent sewage system.[7] It is reported[8] that both amoxicillin and diclofenac cause chronic effects like gastrointestinal and renal tissue damage in many vertebrates, reduction in size, and hatchability among various fish species. Human health can be adversely affected by the consumption of contaminated potable water.[9] Thus, to safeguard the environment from toxicities related to pharmaceutical pollutants, there is a critical requirement of their removal from aqueous sources.

Several remediation strategies have been probed for the uptake of the pharmaceutical-laden wastewater, including solid-phase separation,[10] flocculation, coagulation,[11] ultrasonic degradation,[12] photodegradation,[13] electrochemical degradation,[14] and advanced oxidation processes.[15] These technologies suffer from various flaws as they are technically sophisticated or

Received: October 28, 2019
Accepted: January 23, 2020
Published: February 5, 2020

https://dx.doi.org/10.1021/acsomega.9b03617
ACS Omega 2020, 5, 2843−2855

economically unfavorable. Moreover, they generate toxic effluents and have a limited removal efficacy.[16]

Adsorption offers a prominent method for treating effluents due to its simplicity, economic feasibility, nonproduction of secondary products and free radicals, and high surface area, as well as the presence of functional groups with developed pore assembly.[17] Carbon-based sorbents such as activated carbon derived from olive stones,[18] vine wood,[19] guava seeds,[20] *Moringa oleifera*,[21] pine tree,[22] and Mn-impregnated activated carbon[23] have been ubiquitously used for the uptake of amoxicillin and diclofenac from wastewater. However, due to their high cost[24] and difficulty in separation from aqueous solution, the development of highly effective sorbents is considerably important.

Clay-based hydrogel nanocomposites are envisioned to be potential super adsorbents for the uptake of inorganic and/or organic contaminants from an aqueous solution due to the combining characteristics of both clays and polymers, such as biodegradability, biocompatibility, economic viability, abundance, high specific surface area, three-dimensional network, and swelling−deswelling properties.[25] Recently, many clay-based hydrogel composites have been explored for the confiscation of dyes[26,27] and metals[28−31] mainly because of their chemically reactive functional groups and porous structures. A perusal of the literature reveals that there is little work on the removal of pharmaceutical pollutants by clay−hydrogel nanocomposites; therefore, the main motive was to explore the efficacy of poly(methacrylic acid)/montmorillonite hydrogel (PMA/nMMT) nanocomposite toward the uptake of amoxicillin and diclofenac from wastewater. The nanoscale MMT (nMMT) expectedly with improved cation−exchange capacity, hydrophilicity, adsorption capacity, interactive surface functional groups, and increased surface-to-volume ratio was used as a filler, which could elevate the mechanical strength, increase active sites for maximum sorption, high surface area, and improved regenerative ability of PMA/nMMT nanocomposite. The increase in the adsorption capacity and reusability is crucial from the practical viewpoint. Further, to comprehend the adsorption mechanism, the impact of operative variables such as dose, agitation time, pH, and initial sorbate concentration was explored. Equilibrium data were analyzed using various kinetic and isotherm models and thermodynamic parameters to gain significant insight into the process. The regeneration potential was investigated to probe the sustainability of the synthesized sorbent.

EXPERIMENTAL SECTION

Chemicals and Instruments. Methacrylic acid, montmorillonite (MMT), amoxicillin trihydrate (AMX, 99%), diclofenac sodium (DF, 99%), cetyltrimethylammonium bromide (CTAB), *N*,*N*,*N*,*N*-tetramethylethylenediamine (TEMED), sodium nitrite, 2,2′-bipyridine, ferric chloride, ammonium persulfate (APS), and sodium carbonate were obtained from Merck, India. Sulfanilic acid was procured from CDH and HCl from Fischer Scientific, India. All chemicals/reagents were of A.R grade and used as received. The chemical structures of AMX and DF with their corresponding Fourier transform infrared (FTIR) spectra are depicted in Figure 1.

FTIR spectra of montmorillonite (MMT), nanomontmorillonite (nMMT), poly(methacrylic acid)/montmorillonite hydrogel nanocomposite (PMA/nMMT), and AMX- or DF-loaded nanocomposite were obtained on a PerkinElmer BX FTIR spectrophotometer. X-ray diffraction (XRD) pattern was

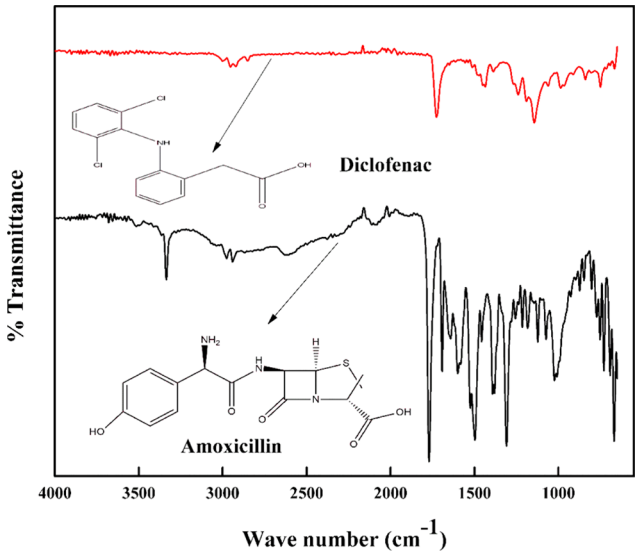

Figure 1. Chemical structures and the corresponding FTIR spectra of AMX and DF.

obtained on a D8 Advance diffractometer (Bruker) with Cu target (λ = 0.154 nm) at 40 kV. X-ray photoelectron spectroscopy (XPS) was done on ESCA+ (Omicron Nanotechnology Oxford Instruments, Germany, Al Kα radiation $h\nu$ = 1486.7 eV). Scanning electron microscopy (SEM) micrographs were obtained on a Phenom ProX (Nanoscience Instruments, Phoenix, AZ) equipped with an energy-disperse X-ray (EDX) instrument under an extra high tension of 15 kV at a working distance of 3.8 mm with an aperture width of 30 μm. Transmission electron microscopy (TEM) images were recorded on a transmission electron microscope (HRTEM 200 kV model, FEI Tecnai). The residual concentrations of AMX and DF at 455 and 520 nm (λ_{max}), respectively, were analyzed by a UV−vis spectrophotometer (T80+, PG Instruments Ltd, U.K.).

Preparation of Nanomontmorillonite Clay (nMMT). Nanomontmorillonite (nMMT) was framed following the procedure illustrated by Khan et al.[31] Briefly, 50 g of MMT was washed three to four times with double-distilled water, left as such overnight and finely grated. This clay (12 g) was dispersed in 100 mL of double-distilled water in a 500 mL beaker containing dil. HCl (4 mL). The mixture was heated at 70 °C on a heating mantle for 30 min and finally dispersed in 50 mL of CTAB (0.5 M) with stirring for 12 h at 70 °C by a magnetic stirrer. The clay was filtered off and dried for 48 h at 80 °C in an oven. Finally, it was ground to nanomontmorillonite (nMMT) powder, which was stored in glass bottles.

Preparation of Poly(methacrylic acid)/Montmorillonite (PMA/nMMT) Hydrogel Nanocomposite. A PMA/nMMT hydrogel nanocomposite was prepared via ultrasound-assisted redox polymerization. Typically, 1.0 g of nMMT was dispersed in 50 mL of distilled water with ultrasonic vibration for 2 h to form a homogeneous dispersion. The ultrasound helps in the improved dispersion of clay, resulting in an enhancement of the mechanical properties and adsorption capacity of the hydrogels. Methacrylic acid monomer (30 mL) was added dropwise to the suspension. Initiator ammonium persulfate (APS) (0.1 M) was added to the mixture followed by 1.0 mL of TEMED accelerator. The dispersion was

https://dx.doi.org/10.1021/acsomega.9b03617
ACS Omega 2020, 5, 2843−2855

vigorously stirred for 4 h at 50 °C by a magnetic stirrer. The resulting sticky mass was acetone-washed and desiccated for 48 h at 70 °C in an oven. The resulting product was ground and stored in a glass bottle. Different nanocomposites were synthesized by varying the nMMT in quantities of 0.5, 1.0, 1.5, and 2.0 g. The nanocomposite prepared using 1.0 g of nMMT depicted better adsorption results than the rest of composites and was therefore used for further adsorption investigation.

Adsorption Studies. Batch mode was employed to investigate the impact of process parameters on the adsorption of AMX and DF onto PMA/nMMT. A fixed mass of PMA/nMMT (0.2−1.8 g) was taken in conical flasks (50 mL) containing 25 mL of a sorbate solution (40−90 mg/L) and shaken on a water bath shaker for 40 min at 303, 313, and 323 K. The impact of the initial solution pH was examined by changing the pH from 2 to 10 by adding NaOH or HCl (0.1 M) solution. When the equilibrium was attained, the solution was centrifuged at 1500 rpm for 5 min, and the residual concentration of AMX or DF in supernatant was spectrophotometrically determined. For absorbance measurement, an equimolar (0.1 M) mixture of HCl, $NaNO_3$, and sulfanilic acid (1.0 mL each) was coupled with Na_2CO_3 (0.1 M, 1.0 mL), and an AMX solution was added to it, which developed an orange-colored solution[32] with λ_{max} at 455 nm. The DF solution was treated with a $FeCl_3$ solution (0.1 M, 1.0 mL) and then subsequently reacted with 2,2′-bipyridine (0.1 M, 1.0 mL) to form a red solution,[33] which absorbed at 520 nm (λ_{max}). The parameters of sorption capacity, q_e, and removal efficiency (%), were assessed using eqs 1 and 2, respectively

$$q_e = \left[\frac{C_i - C_e}{W_M} \times V\right] \quad (1)$$

$$\text{removal efficiency}(\%) = \left[\frac{C_i - C_e}{C_i} \times 100\right] \quad (2)$$

where C_e and C_i are the equilibrium and initial sorbate concentrations (mg/L), V represents volume (L) of sorbate solution, and W_M is the sorbent mass (g). Isotherm studies were investigated by shaking 25 mL (40−90 mg/L) of sorbate solution with PMA/nMMT (1.2 or 1.4 g for AMX or DF) for 40 min at 303, 313, and 323 K. The kinetic investigations were accomplished by shaking 25 mL (60−80 mg/L) of sorbate solution with PMA/nMMT (AMX: 1.2 g; DF: 1.4 g) for 40 min at 323 K.

RESULTS AND DISCUSSION

Characterization of PMA/nMMT Hydrogel Nanocomposite. The binding of pollutants is determined by the existence of functional groups on the surface of the adsorbent. Thus, the FTIR technique was employed to verify the chemical functionality. The FTIR spectra of MMT, nMMT, PMA/nMMT, and AMX- or DF-loaded PMA/nMMT are compared in Figure 2. A broad peak at 3440 cm^{-1} and a sharper one at 1637 cm^{-1} correspond to the O−H stretching and deformation vibrations, respectively.[34] The peak at 3631 cm^{-1} is assigned to O−H stretching vibrations of the Si−OH and Al−OH groups of montmorillonite.[35] The absorption band observed at 1031 cm^{-1} is attributed to in-plane stretching vibrations of the Si−O group,[36] whereas the peaks at 528 and 455 cm^{-1} represent Al−O−Si and Si−O−Si bending vibrations, respectively.[37] The absorption bands in nMMT at

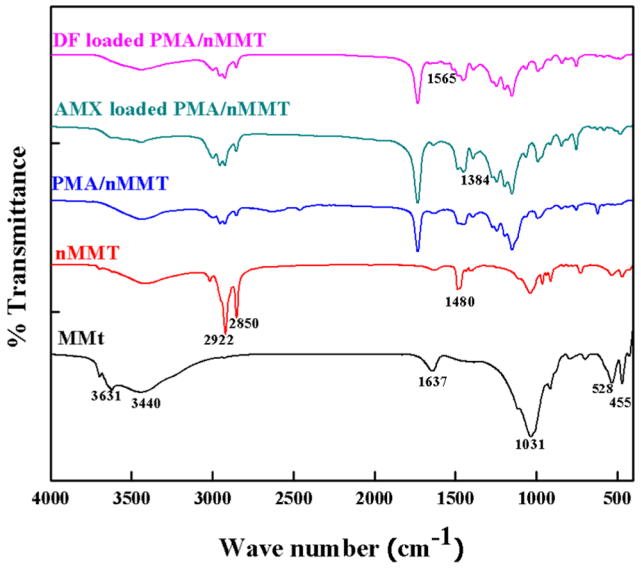

Figure 2. FTIR spectra of MMT, nMMT, PMA/nMMT hydrogel nanocomposite, and AMX- and DF-loaded nanocomposite.

2922 and 2850 cm^{-1} represent stretching modes of the CH_3 and CH_2 groups of CTAB.[38] Moreover, the C−C−C flexural vibration of the methylene group associated with the cetyltrimethylammonium ion peak is exhibited at 1480 cm^{-1}, which confirms the successful modification of montmorillonite. The reduction in the intensity of absorption peaks in the PMA/nMMT spectrum at 2922 and 2850 cm^{-1} along with the appearance of new sharp peaks at 1730 and 1252 cm^{-1} corresponding to C═O and C−O stretching vibrations of the carboxylic group[39] supports the formation of hydrogel nanocomposite. In the spectra of PMA/nMMT-loaded AMX and DF, the appearance of characteristic absorption bands corresponding to the C−N stretching of the amine group (1384 cm^{-1}) and the O−C═O stretching of the carboxylic group (1565 cm^{-1}) reveals the successful sorption of AMX and DF onto PMA/nMMT. A red shift from 3440 to 3454 cm^{-1} indicates the participation of the −OH group in hydrogen bonding during the sorption process. The structural vibration regions of PMA/nMMT show no significant changes after sorption, depicting the structural stability of PMA/nMMT after AMX and DF sorption.

XRD diffractograms of MMT, nMMT, and PMA/nMMT are displayed in Figure 3. MMT having a 2:1 layered structure of smectite class is represented by a sharp peak at 2θ = 26.80° corresponding to quartz mineral,[41] while the peak at 2θ = 19.82° confirms the presence of random stacked layers. The basal (001) space of MMT is displayed at 2θ = 6.29°. The diffractogram of nMMT exhibits a change in peak intensities attributed to structural modifications in existing planes with the formation of new layers. Moreover, the average crystallite sizes (L) of MMT and nMMT using Scherer's equation ($L = 0.9\lambda/\beta \cos\theta$) were 103.3 and 55.3 nm, respectively. The diffractogram pattern of PMA/nMMT displays an amorphous halo at 14.29°. The disappearance of the basal peak indicates exfoliation of nMMT layers into the PMA matrix,[42] which suggests the formation of the PMA/nMMT hydrogel nanocomposite.

The chemical states of PMA/nMMT, before and after adsorption of AMX and DF, were analyzed by XPS, and are depicted in Figure 4. The study illustrates the existence of C,

https://dx.doi.org/10.1021/acsomega.9b03617
ACS Omega 2020, 5, 2843−2855

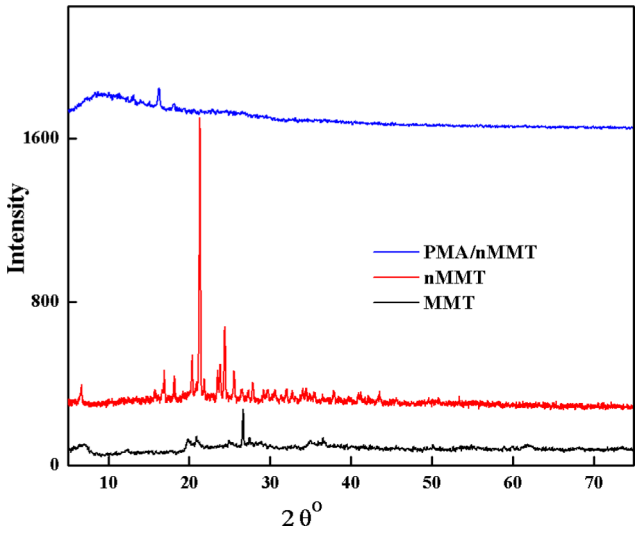

Figure 3. XRD spectra of MMT, nMMT, and PMA/nMMT hydrogel nanocomposite.

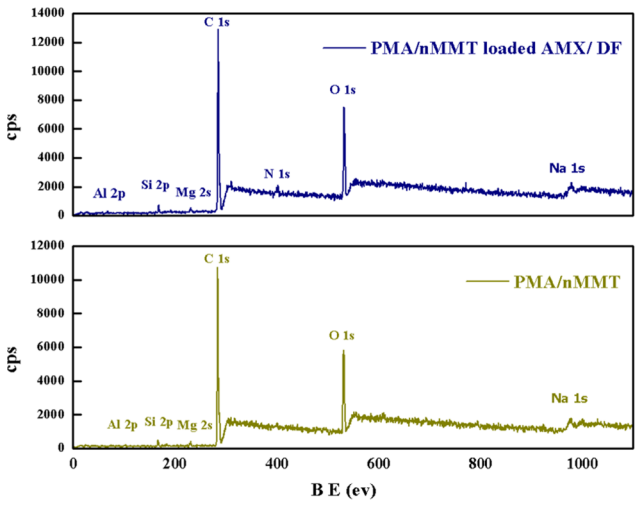

Figure 4. XPS spectra of PMA/nMMT hydrogel nanocomposite and AMX-/DF-loaded nanocomposite.

O, Al, Si, and Mg in the hydrogel nanocomposite. The C 1s peak is assigned to the presence of PMA, while the peaks of Si 2p, Al 2p, and Mg 2s are attributed to MMT.[43] The peak of Na 1s determines the presence of sodium on the MMT surface. The O 1s peak is due to both PMA and MMT. The presence of N 1s peak and an increase in carbon and oxygen intensities in the spectra of PMA/nMMT after sorption depict the successful grafting of AMX or DF onto the surface of PMA/nMMT.

The SEM micrographs recorded at a magnification of 1.00 KX along with the EDX of MMT, nMMT, PMA/nMMT, and AMX- or DF-loaded PMA/nMMT are illustrated in Figure 5. It is observed that raw MMT owes a layered sheet structure showing the presence of larger grains. After modification, the sheets of MMT are exfoliated into tiny particles, which may be due to the elimination of Si^{2+} and Al^{3+} from the octahedral sites. The EDX spectrum of nMMT exhibits a high percentage of carbon, which may primarily be due to the surfactant utilized for modification as the main constituent of CTAB ($C_{19}H_{42}BrN$) is carbon (84%). PMA/nMMT displays a coherent and near-co-continuous structure. Further, no pores are visible, which depicts the complete exfoliation of nMMT into the PMA matrix. After AMX or DF sorption, changes in the PMA/nMMT morphology are observed. The surface becomes asymmetric with an increase in the rough texture.

TEM investigation was used to assess the structural insights of nMMT and PMA/nMMT. The TEM micrographs of nMMT shown in Figure 6a exhibit nearly spherical particles of 7−15 nm diameter. The presence of CTAB in the interlamellar space of nMMT prevents its agglomeration to a large extent. The TEM images of PMA/nMMT (Figure 6b) display a PMA network shown as the light zone in which nMMT as the dark zone is uniformly dispersed.

Effect of Operational Parameters. To figure out the impact of sorbent dosage on the removal efficiency, different varying amounts (0.2−1.4 g/L) of PMA/nMMT were used. With increasing sorbent dose, a sharp escalation in the removal efficiency for AMX (74.3−98.6%) and DF (75.8−96.0%) is observed, which can be credited to an overall increase in the sorbent surface regions. However, a fall in the adsorption capacity for AMX occurs from 111.5 to 20.6 mg/g and for DF from 151.7 to 27.4 mg/g (Figure S6). This antagonistic effect could be associated with the aggregation of sorbent at higher doses, which enlarges the diffusional pathway for AMX and DF to reach the binding sites.[44] Therefore, the optimized dose for AMX (1.2 g/L) and DF (1.4 g/L) at which maximum removal was attained when the pollutant concentration was 40 mg/L was taken for subsequent experiments.

Contact time is a prime factor that affects the adsorption process. To illustrate the impact of contact time on the adsorption of AMX and DF onto PMA/nMMT, experiments were conducted for 10−60 min with a 10 min time interval, keeping the concentration (40 mg/L) and sorbent dose (1.2 and 1.4 g/L for AMX and DF, respectively) constant. It can be inferred from Figure S7 that the increase in the uptake efficiency within the initial 40 min is rapid but exhibits a steady trend with further increase in time, which may be attributed to the occurrence of available sorption sites on the sorbent during the initial stage of the sorption process and the increase in the collision frequency of AMX or DF on the surface of PMA/nMMT. The maximum % efficacy and sorption capacity is achieved at 40 min, which is subsequently used in further investigations. The scavenging potential of PMA/nMMT (95.80% for AMX and 95.14% for DF) within a time period of 40 min qualifies it as a potential sorbent.

The pH of the reaction environment is a critical aspect that governs the protonation and deprotonation of pollutants in the aqueous phase, which affects pollutant binding onto the sorbent surface. To determine the effect of initial solution pH on the sorption of AMX and DF on the PMA/nMMT surface, pH was changed from 2 to 10 (Figure 7), keeping rest of the parameters such as contact time (40 min), dose (1.2 and 1.4 g/L for AMX and DF, respectively), and initial concentration (40 mg/L) constant. It is evident that AMX contains three functional groups with different pK_a values—carboxyl (pK_a = 2.68), amine (pK_a = 7.49), and hydroxyl (pK_a = 9.63), which means AMX is cationic at pH < 2.68, anionic at pH > 7.49, and zwitterionic at neutral pH.[45] At pH 2, cationic exchange takes place between positively charged AMX and the sorbent as pH_{pzc} of PMA/nMMT is 3.98.[46] When the pH is increased from 3 to 4, stronger electrostatic interactions between negatively charged amoxicillin and positive PMA/nMMT surface are observed, escalating the removal efficiency. As the solution pH is increased further, AMX becomes neutral and is

https://dx.doi.org/10.1021/acsomega.9b03617
ACS Omega 2020, 5, 2843−2855

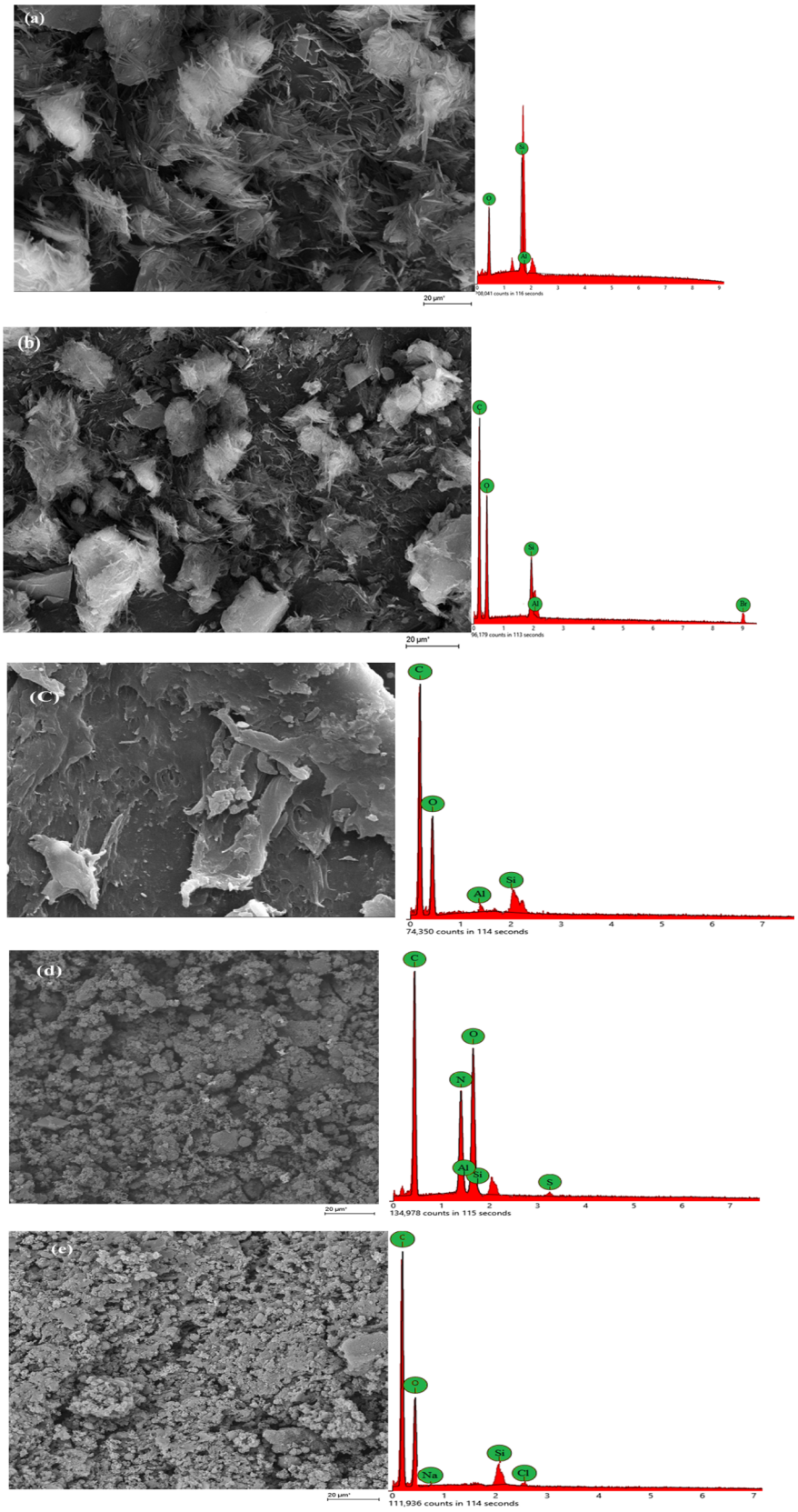

Figure 5. SEM–EDX micrographs of (a) MMT, (b) nMMT, (c) PMA/nMMT, and (d) AMX- and (e) DF-loaded nanocomposite.

adsorbed onto the surface of PMA/nMMT by the partition mechanism. Further increase in pH increases the electrostatic repulsion, thereby decreasing the adsorption.[47] The removal efficiency of DF is quite high at acidic pH and falls off with increasing pH. At pH < pK_a (4.2), the DF becomes neutral[48] and the PMA/nMMT surface is positive; therefore, instead of electrostatic attraction, the hydrogen bonding may dominate the removal mechanism.

https://dx.doi.org/10.1021/acsomega.9b03617
ACS Omega 2020, 5, 2843−2855

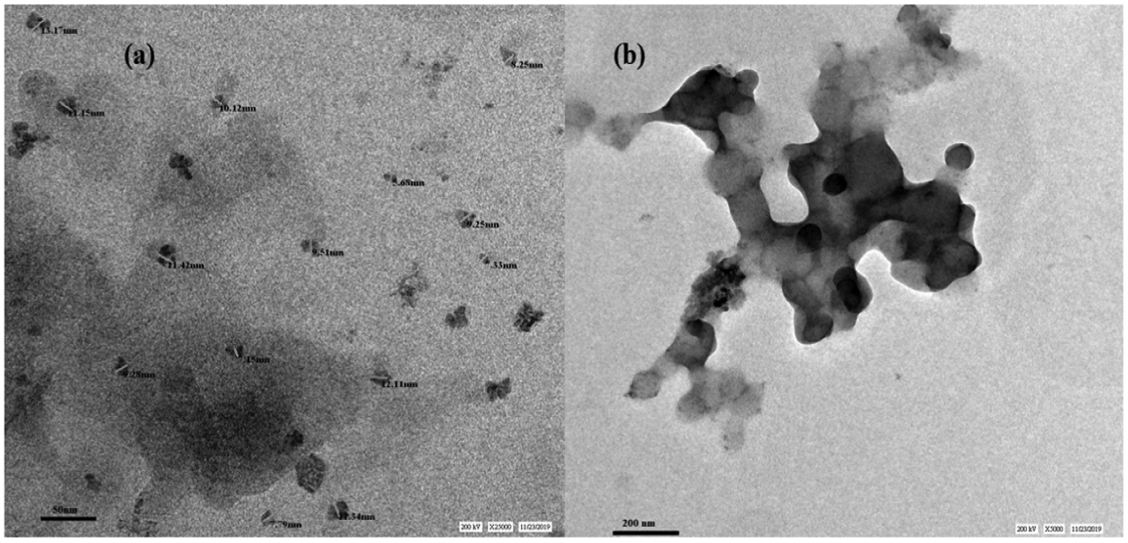

Figure 6. TEM micrographs of (a) nMMT and (b) PMA/nMMT.

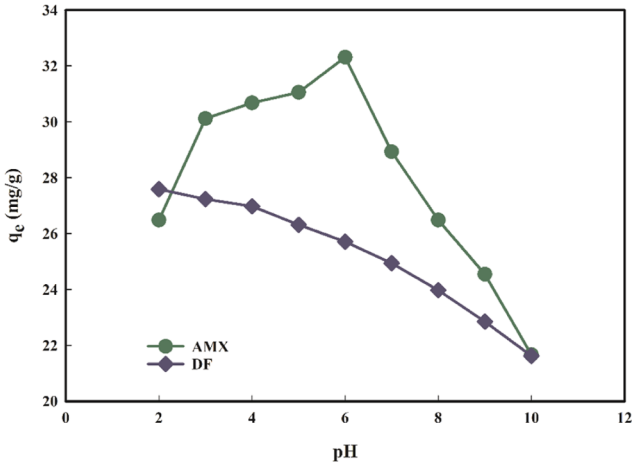

Figure 7. Effect of pH on (a) AMX and (b) DF removal.

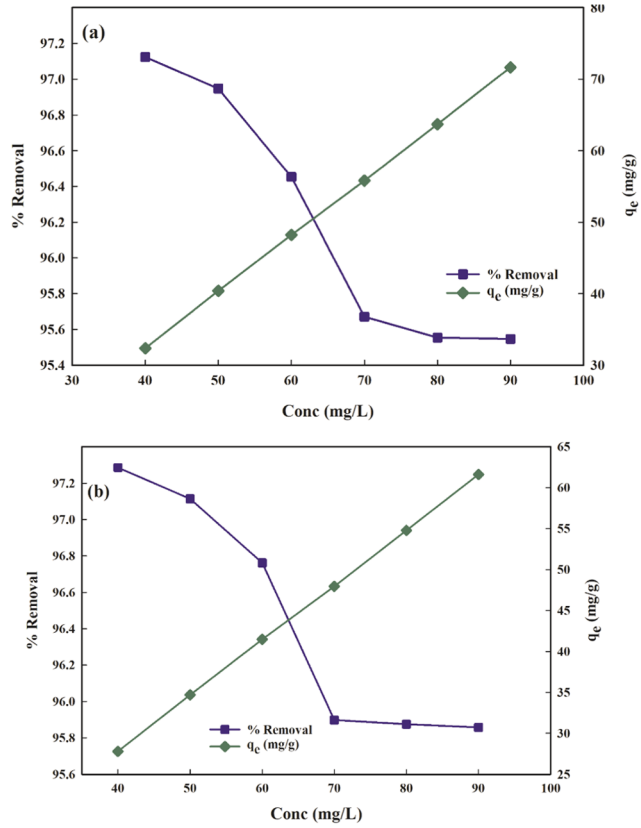

Figure 8. Effect of Initial concentration for (a) AMX and (b) DF removal.

The effect of the initial concentration of pollutants on the removal efficacy of PMA/nMMT for the uptake of AMX and DF is shown in Figure 8. It reveals that with an increase in the initial sorbate concentration from 40 to 90 mg/L, an escalation in the sorption capacity for AMX (from 32.37 to 71.66 mg/g) and DF (from 27.29 to 61.62 mg/g) may be accredited to a large driving force provided by higher initial concentration that reduces the mass transfer resistance, leading to an increase in the adsorption amount.[49] Also, at the initial stage, both the pollutants adhere conveniently on the PMA/nMMT surface due to the availability of active sites, which boosts the sorption capacity till equilibrium is attained. At a low concentration, the relative number of active sites and sorbate molecules is high, which makes the sorbate molecules interact with the sorbent and results in prompt uptake from the solution. On increasing the concentration, the removal efficacy represents a fall attributed to the saturation of binding sites.

Adsorption Isotherm Studies. Adsorption isotherm is a fundamental tool that illuminates the interaction between sorbate and sorbent and further describes the maximum sorption capacity. To design the process and to figure out the best-fit model, the nonlinear form of various isotherm models was coordinated with equilibrium data at 303, 313, and 323 K. Besides, the applicability of isotherm models was appraised based on correlation coefficient (R^2) and standard error of estimation (SEE) that were calculated for each model and are presented in Table 1.

The Langmuir model presumes adsorption to occur via monolayer formation on the homogeneous surface.[50] It further assumes that active sites are finite and no lateral interaction is observed between the adsorbed molecules on adjacent sorption sites. Equation 3 expresses nonlinear regression of the Langmuir model

https://dx.doi.org/10.1021/acsomega.9b03617
ACS Omega 2020, 5, 2843−2855

Table 1. Isotherm Parameters

		AMX			DF		
isotherm	isotherm constant	303 K	313 K	323 K	303 K	313 K	323 K
Langmuir	Q_m	119.07	130.37	152.65	137.15	146.25	152.86
	b	0.285	0.305	0.295	0.151	0.184	0.139
	R_L	0.055	0.051	0.053	0.086	0.072	0.093
	R^2	0.983	0.989	0.992	0.981	0.985	0.992
	SEE	1.869	1.531	1.309	1.954	1.515	1.392
Freundlich	K_f	28.91	32.06	35.53	20.02	20.44	24.22
	$1/n_f$	0.564	0.595	0.653	0.680	0.689	0.694
	R^2	0.990	0.991	0.994	0.988	0.992	0.996
	SEE	1.659	1.362	0.135	1.317	0.887	0.790
Temkin	K_t	2.50	2.67	2.81	1.67	1.68	2.10
	b_t	0.091	0.086	0.080	0.094	0.093	0.091
	R^2	0.977	0.985	0.988	0.962	0.968	0.971
	SEE	2.189	1.776	1.584	2.692	2.494	2.377
D−R	q_D	98.71	106.89	118.70	92.41	97.30	99.44
	E	1.26	1.35	1.42	1.10	1.14	1.28
	R^2	0.972	0.986	0.988	0.958	0.967	0.973
	SEE	2.570	1.954	1.606	2.833	2.517	2.284

$$q_e = \frac{Q_{max} b C_e}{(1 + bC_e)} \quad (3)$$

where C_e (mg/L) is the equilibrium concentration of sorbate in solution, b (L/mg) is the Langmuir binding constant, q_e and Q_{max} (mg/g) are the amount of sorbate adsorbed at equilibrium and the maximum sorption capacity, respectively.

The values of Q_{max}, b, and R^2 were investigated from the plot of q_e vs C_e at 303−323 K (Figure S1). An increment in b values with a rise in temperature depicts a stronger interaction between sorbent and sorbate. The Q_{max} values turn out to be 152.65 mg/g for AMX and 152.86 mg/g for DF, which are significantly higher than those of reported sorbents (Table 2).

Table 2. Comparison of Q_{max} (mg/g) Values

sorbate	sorbent	Q_{max} (mg/g)	reference
amoxicillin	CS-Fe/Ni	29.63	51
	O-clays	33.51	40
	O-MMT	48.6	52
	modified bio-hydrochar	92.87	53
	magnetic graphene nanoparticles	106.38	47
	Mn-impregnated activated carbon	131.57	23
	PMA/nMMT	152.65	this work
diclofenac	MWCNT	4.18	54
	PPhA	21.11	55
	CTAB-ZIF-76	60.58	56
	Terminalia catappa fruit shell	96.1	57
	coconut shell activated carbon	103.0	58
	orange peel activated carbon	144	59
	PMA/nMMT	152.86	this work

This observation establishes the superiority of PMA/nMMT nanocomposite over many other sorbents for AMX and DF removal. The enhancement in maximum sorption capacity with the rise in temperature is indicative of the endothermic nature of the process. Thus, at a higher temperature, more energy is supplied, which augments the physical attachment of sorbate on the binding sites of the sorbent. The values of separation factor, $R_L = \frac{1}{1 + bC_o}$ (0.053 for AMX and 0.093 for DF), illustrate the sorption process to be favorable.

The Freundlich model elucidates the multilayer sorption pattern onto the heterogenous surface.[60] The nonlinear form is described by eq 4

$$q_e = (K_f C_e)\frac{1}{n_f} \quad (4)$$

where K_f (L/mg) attributes to the Freundlich constant associated with the sorption capacity and $1/n_f$ is the heterogeneity factor, which depicts whether adsorption is favorable ($1/n_f < 1$) or unfavorable ($1/n_f > 1$). The parameters K_f and $1/n_f$ were assessed from the plot of q_e vs C_e (Figure 9), which suggests the isotherm to be favorable as the values of $1/n_f$ (0.56−0.65 for AMX and 0.68−0.69 for DF) are less than unity (Table 1). The values of $1/n_f$ may be due to the surface site distribution, which limits the sorbate−sorbent interaction with an increase in surface density.

Temkin isotherm speculates reduction in the heat of adsorption of all molecules in the layer with increased sorbent−sorbate interaction and further specifies the uniform distribution of binding energies. Equation 5 expresses the nonlinear form of the Temkin isotherm model

$$q_e = \beta_t \ln(K_t C_e) \quad (5)$$

where K_t (L/g) is the binding constant related to the maximum binding energy and b_t ($=RT/\beta_t$) is a constant relevant to heat of adsorption (kJ/mol). The values of K_t and b_t were calculated from the q_e vs C_e plot (Figure S2), which depicts a significant sorbate−sorbent interaction and a minor change in the heat of sorption with temperature change, respectively. The obtained values of b_t (Table 1) substantiate the physisorption to dominate the sorption process.

The D−R isotherm is a generalized model that is not restricted to the homogeneous surface or constant adsorption potential.[61] This model differentiates between physical and chemical adsorption because of the mean energy of adsorption (E). It is reported[62] that if the value of E (kJ/mol) is between 1 and 8 kJ/mol, then the physical interaction dominates the adsorption process and an ion-exchange phenomenon is

https://dx.doi.org/10.1021/acsomega.9b03617
ACS Omega 2020, 5, 2843−2855

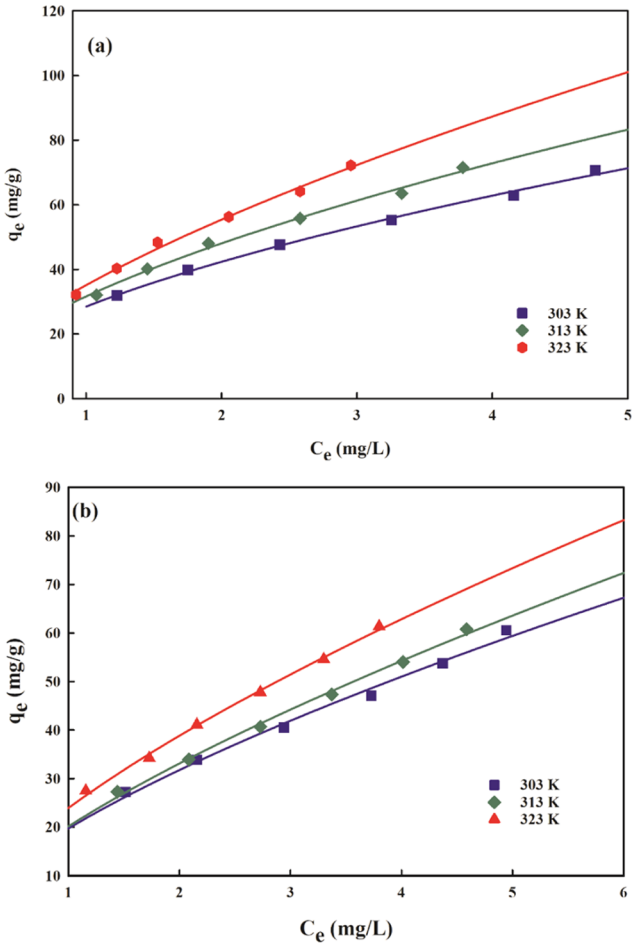

Figure 9. Freundlich isotherm plot for (a) AMX and (b) DF removal.

observed between 8 and 16 kJ/mol, and above 16 kJ/mol, chemical interaction is the main force. Equation 6 enunciates the nonlinear equation of the D−R model

$$q_e = q_D \exp\left[-K_D\left\{\ln\left(1 + \frac{1}{C_e}\right)^2\right\}\right] \quad (6)$$

where q_D (mg/g) is the D−R constant and K_D ($=\beta_{ad}R^2T^2$) corresponds to the activity coefficient. Isotherm parameters were determined from the plots of q_e vs C_e (Figure S3). The mean adsorption energy was calculated using $E = \frac{1}{\sqrt{2\beta_{ad}}}$. The value of adsorption energy (E) for AMX (1.26−1.42 kJ/mol) and DF (1.10−1.28 kJ/mol) falls in the range of physisorption (1−8 kJ/mol) supporting the findings of the Temkin model.

To analyze the best-fit model, statistical parameters such as correlation coefficient (R^2) and standard error of estimation (SEE) were utilized (Table 1). Higher R^2 values (0.994 for AMX and 0.996 for DF) and lower SEE values (0.135 for AMX and 0.790 for DF) verify that the Freundlich model best describes the equilibrium data implying multilayer sorption of AMX and DF on the heterogeneous surface of PMA/nMMT.

Kinetic Investigations. Adsorption rate is a prime factor that determines the adsorption efficiency of an adsorbent. It illustrates the mechanism of control of the sorption process, which may be surface adsorption, chemical reaction, or penetration mechanism. The kinetics of AMX and DF adsorption onto PMA/nMMT was evaluated by pseudo-first-order and pseudo-second-order models. Nonlinear forms of the models are expressed as (eqs 7 and 8)

$$q_t = q_e(1 - e^{-k_1 t}) \quad (7)$$

$$q_t = \frac{(k_2 q_e^2 t)}{(1 + k_2 q_e t)} \quad (8)$$

where k_1 (1/min) and k_2 (g/(mg min)) correspond to rate constants of pseudo-first-order and pseudo-second-order models, respectively. The values of q_e, k_1, and k_2 (Table 3) of pseudo-first-order (Figure S4) and pseudo-second-order rate equations (Figure 10) were determined from the plot of q_t vs t. It is inferred that the pseudo-second-order model provides the best representation of sorption kinetics based on higher R^2 (AMX: 0.96; DF: 0.97) and lower SSE values (AMX: 0.48−0.58; DF: 0.34−0.37), which implies that the sorption rate of PMA/nMMT is influenced by the number of binding sites rather than the concentration of AMX or DF in solution. Moreover, the k parameter has a relatively higher value, which qualifies PMA/nMMT as a rapid scavenger of AMX or DF from the aqueous phase.

Diffusion models were further related with equilibrium data to elucidate the diffusion mechanism and the rate-controlling step. The adsorption kinetics usually involves four steps: (a) mass transfer of sorbate from bulk solution to the external surface of sorbent (film diffusion), (b) boundary layer diffusion, (c) mass movement of sorbate from the external layer into interior pores of the sorbent (intraparticle diffusion), and (d) coverage of all binding sites by adsorbate.[63] The boundary layer and coverage of active sites have a meager impact, while film diffusion and intraparticle diffusion affect the kinetics considerably.

Generally, the intraparticle diffusion model[64] based on surface and pore diffusion is utilized to determine the rate-controlling step. It is expressed in the mathematical form as (eq 9)

Table 3. Kinetic Parameters

		pseudo-first-order					pseudo-second-order			
sorbate	concn (mg/L)	k_1 (1/min)	R^2	SEE	q_e (cal) (mg/g)	q_e (exp) (mg/g)	$k_2 \times 10^{-2}$ (g/(mg min))	q_e (cal) (mg/g)	R^2	SEE
AMX	60	0.233	0.66	1.205	48.15	48.22	0.012	50.20	0.94	0.485
	70	0.240	0.71	1.341	55.76	55.80	0.012	57.98	0.95	0.552
	80	0.245	0.74	1.386	63.32	63.70	0.011	65.70	0.96	0.581
DF	60	0.245	0.72	0.939	40.93	41.46	0.017	42.49	0.95	0.377
	70	0.253	0.75	0.918	47.17	47.94	0.016	48.79	0.96	0.346
	80	0.255	0.76	1.001	53.69	54.78	0.014	55.50	0.97	0.343

https://dx.doi.org/10.1021/acsomega.9b03617
ACS Omega 2020, 5, 2843−2855

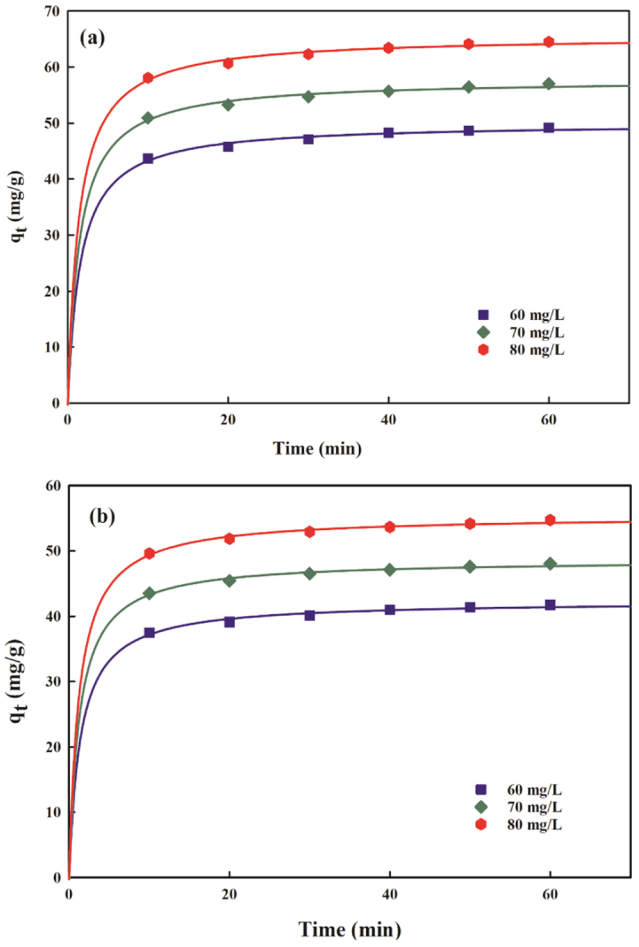

Figure 10. Pseudo-second-order kinetics plot for (a) AMX and (b) DF removal.

$$q_t = K_i t^{0.5} + C_i \quad (9)$$

where K_i (mg/(g min$^{0.5}$)) implies the intraparticle rate constant and C_i is a constant related to the thickness of the boundary layer. The values of K_i and C_i were determined from the slope and intercept, respectively, of q_t vs $t^{0.5}$ plots, and are presented in Table 4. It is evident from the plots that mainly three steps are involved in AMX and DF sorption onto PMA/nMMT. The initial portion portrays immediate sorption on the external surface. The gradual coverage of active sites due to intraparticle diffusion of AMX and DF is represented by the second stage. The decrease in the intraparticle diffusion rate due to extremely low sorbate concentration and lower availability of active sites is described by the final step.[65] As described by eq 9, if the plot of q_t vs $t^{0.5}$ is linear and passes through the origin, intraparticle diffusion dominates the sorption kinetics. However, the plots exhibit multilinearity and deviate from the origin (Figure 11), which implies that intraparticle diffusion is not the sole rate-limiting step. Moreover, larger values of the intercept for AMX (40.39−54.29) and DF (34.99−46.81) reveal a greater boundary layer effect.[66]

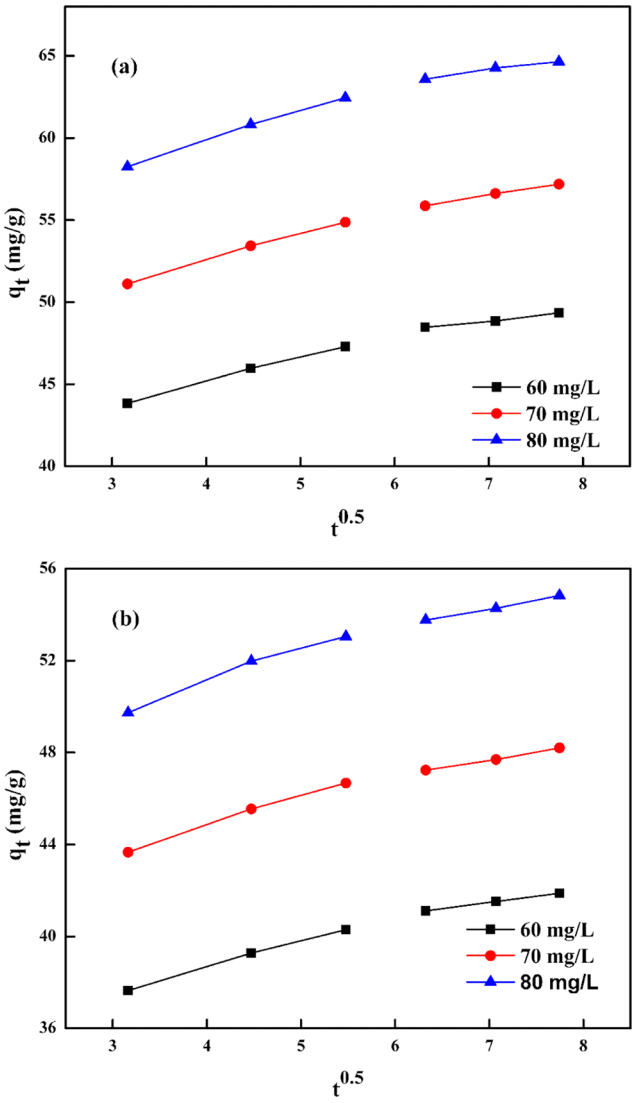

Figure 11. Intraparticle diffusion plots for (a) AMX and (b) DF removal.

The Boyd kinetic model[67] was further employed to appraise kinetic data, which is expressed as (eq 10)

Table 4. Diffusion Parameters

		intraparticle diffusion				liquid-film diffusion		
sorbate	concn (mg/L)	K_i (mg/(g min$^{0.5}$))	C_i	R^2	SEE	K_A (1/min)	R^2	SEE
AMX	60	1.209	40.39	0.96	0.605	0.061	0.98	0.003
	70	1.320	47.30	0.97	0.528	0.058	0.97	0.004
	80	1.407	54.29	0.95	0.758	0.069	0.96	0.006
DF	60	0.927	34.99	0.97	0.428	0.061	0.98	0.039
	70	0.962	41.00	0.95	0.529	0053	0.99	0.016
	80	1.073	46.81	0.95	0.609	0.053	0.99	0.014

https://dx.doi.org/10.1021/acsomega.9b03617
ACS Omega 2020, 5, 2843−2855

$$-\ln(1 - F) = K_A t \quad (10)$$

where F (q_t/q_e) represents the fractional equilibrium, K_A (1/min) is the liquid-film diffusion constant. The deviation of the straight-line plots of $-\ln(1 - F)$ vs t (Figure S5) from the origin represents that the liquid-film diffusion is not the sole controlling step,[68] which illustrates both intraparticle and liquid-film models governing the diffusive mechanism.

Thermodynamic Investigations. Comprehensive information regarding innate energy changes associated with the adsorption process is specified by thermodynamic parameters. The standard enthalpy change (ΔH°), standard entropy change (ΔS°), and standard Gibbs free-energy change (ΔG°) were analyzed at 303, 313, and 323 K, and the values are provided in Table 5. The thermodynamic parameters were

Table 5. Thermodynamic Parameters

sorbate	concn (mg/L)	ΔH° (kJ/mol)	ΔS° (kJ/(mol K))	$-\Delta G^\circ$ (kJ/mol)		
				303 K	313 K	323 K
AMX	50	20.06	0.083	5.22	6.06	6.89
DF	50	18.83	0.081	5.70	6.51	7.32

determined using the van't Hoff plot of $\log(q_e/C_e)$ vs $1/T$ (Figure 12) employing eq 11 and Gibbs equation (eq 12)

$$\log\left(\frac{q_e}{C_e}\right) = \frac{\Delta S^\circ}{2.303R} - \frac{\Delta H^\circ}{2.303RT} \quad (11)$$

$$\Delta G^\circ = \Delta H^\circ - T\Delta S^\circ \quad (12)$$

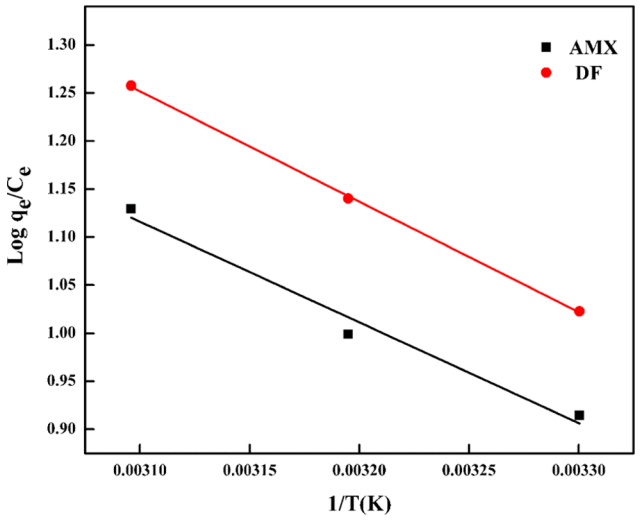

Figure 12. van't Hoff plots.

where R (8.314 J/(K mol)) represents the ideal gas constant and T (K) is the absolute temperature. The ΔG° values are found to be negative at all studied temperatures for AMX (−5.22, −6.06, and −6.89) and DF (−5.70, −6.51, and −7.32), confirming the feasibility and spontaneity of the sorption process. The positive values of ΔS° demonstrate an increase in the disorder of AMX (0.083 kJ/mol) and DF (0.081 kJ/mol) molecules at the sorbate−sorbent interface. The ΔH° values for AMX (20.06 kJ/mol) and DF (18.83 kJ/mol) specify the endothermic nature of sorption on the surface of PMA/nMMT.

Simultaneous Removal of AMX and DF and the Effect of NaCl on % Sorption by the PMA/nMMT Nanocomposite. Simultaneous sequestration of pollutants specifies the portion of binding sites occupied by each of the pollutants on the surface of sorbent.[69] It further evaluates the interaction of one sorbate on the sorbent surface in the companionship of other sorbate molecules. To investigate the simultaneous sorption, a binary system of AMX-DF with an initial concentration of 40−90 mg/L and PMA/nMMT (1.5 g/L) was shaken for 40 min on a water bath shaker. Equation 13 was utilized to calculate the ratio of % removal efficiencies

$$R = q_a/q_m \quad (13)$$

where q_a and q_m are the removal efficiencies of AMX and DF in the binary system and monocomponent system with the same initial concentration, respectively. Simultaneous sorption process might fall under three cases based on the values of R. If $R > 1$, a synergistic effect is observed, i.e., both the sorbate molecules work in association that results in an escalation in % removal. If $R < 1$, the antagonistic effect is dominant, which implies the suppression of one pollutant in the presence of other, which leads to a decrease in the removal efficacy. If $R = 1$, no interaction can be seen, which means that % removal is independent of the impact of binary mixture.[70] In this work, the antagonistic effect was observed as R values are less than unity (Figure 13a), which suggests that competitive sorption is prevalent between both the drugs.

The salinity of the solution has a prominent impact on the adsorption process. To illustrate the effect of Cl^- on % sorption of AMX and DF, NaCl solutions of varying concentrations (0.1, 0.5, 0.7, 1.0, 1.5 M) were used. Figure 13b demonstrates that both pharmaceutical contaminants exhibit a monotonic decrease in % removal with the rise in salinity. The observed trend may be due to the competitive sorption of sorbate and the ions from the solution onto the available binding sites on the PMA/nMMT surface. This validates the electrostatic interaction as the main mechanism for sequestration, which is consistent with the pH investigations.

Desorption and Reusability of Adsorbent. Long-term reusability and ease in the recovery of the sorbent is a critical factor for its industrial application as it has a significant impact on economic conceivability and reduces the disposal problem of the used sorbent. The reusability potential of PMA/nMMT was assessed by performing four desorption−adsorption cycles. PMA/nMMT (2 g/L) was saturated with AMX and DF (60 mg/L) for 3 h and then dried. Sorption sites were regenerated using HCl (0.1 M). The sorbent exhibits a better regeneration potential for AMX and DF up to four cycles (Table 6), which signifies PMA/nMMT as a potential sorbent. The removal efficiency diminishes owing to unadsorbed pollutants and weight loss of PMA/nMMT during the sorption−desorption cycles.

CONCLUSIONS

This work demonstrated the successful preparation of a poly(methacrylic acid)/montmorillonite hydrogel nanocomposite via redox polymerization and its subsequent usage in AMX and DF uptake from the aqueous phase. The structural characteristics of PMA/nMMT were investigated employing FTIR, XRD, XPS, scanning electron microscopy−energy dispersive X-ray spectroscopy (SEM−EDS), and TEM

https://dx.doi.org/10.1021/acsomega.9b03617
ACS Omega 2020, 5, 2843−2855

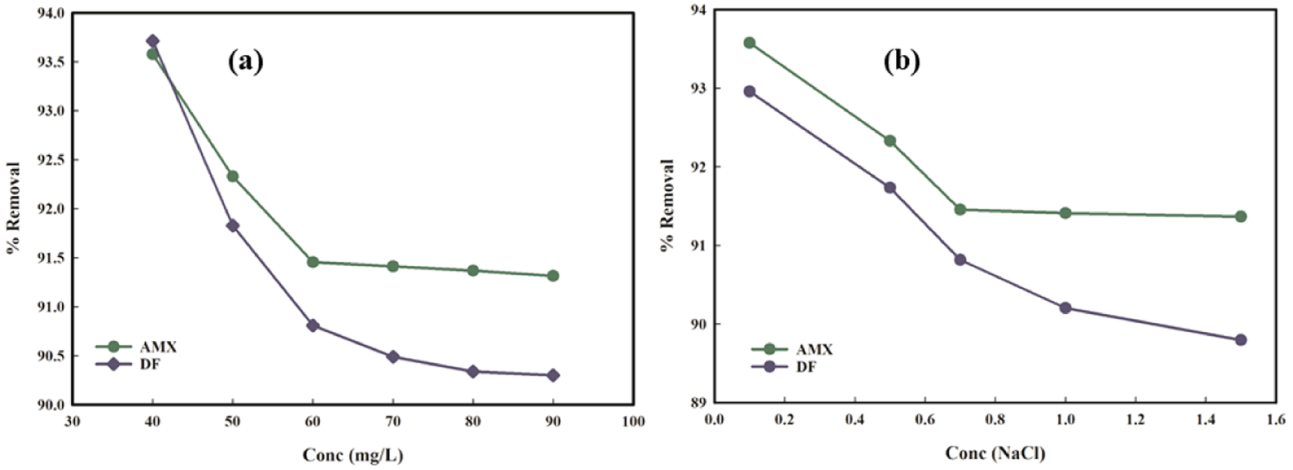

Figure 13. Effect of (a) simultaneous sorption and (b) NaCl on AMX and DF sorption.

Table 6. Sorption−Desorption Cycle

regeneration cycle	% sorption AMX	% desorption AMX	% sorption DF	% desorption DF
1	87.34	91.24	88.42	91.34
2	80.20	85.14	80.45	82.36
3	71.16	75.16	70.21	71.97
4	63.53	64.49	61.88	62.03

techniques. The impact of operative variables was evaluated, and the optimal conditions were found to be dose (1.2 g/L for AMX and 1.4 g/L for DF), agitation time (40 min), pH (6 for AMX and 2 for DF), and initial concentration (80 mg/L). Various isotherm models were utilized, among which the Freundlich model appropriately suited the equilibrium data, suggesting multilayer adsorption onto the heterogeneous surface. The maximum sorption capacity was found to be 156.65 for AMX and 152.86 mg/g for DF, which is better than most of the reported sorbents establishing the high performance of PMA/nMMT hydrogel nanocomposite. The adsorption kinetics was dominated by pseudo-second order with both intraparticle and film diffusion controlling the rate. The synergistic effect of cationic exchange, electrostatic interaction, partition mechanism, and hydrogen bonding could elucidate the enhanced adsorption of AMX and DF onto PMA/nMMT. Thermodynamic parameters revealed that AMX and DF sorption onto PMA/nMMT was spontaneous and endothermic in nature, and the sorption capacity increased with rising temperature. The process was accompanied by an increase in randomness at the solid−solution interface, which was specified by positive ΔS° values. The sorbent exhibited a better reusability potential up to four cycles without a considerable loss in its efficiency. Simultaneous sorption and presence of NaCl limits the removal efficiency of PMA/nMMT. Therefore, facile fabrication, economic feasibility, and better sorption capacity coupled with reusability authenticate PMA/nMMT as a potential sorbent for AMX and DF removal from the aquatic environment.

■ ASSOCIATED CONTENT

Supporting Information

The Supporting Information is available free of charge at https://pubs.acs.org/doi/10.1021/acsomega.9b03617.

Langmuir isotherm plots (Figure S1); Temkin isotherm plots (Figure S2); D−R isotherm plots (Figure S3); pseudo-first-order plots (Figure S4); liquid-film diffusion plots (Figure S5); effect of adsorbent dose (Figure S6); and effect of contact time (Figure S7) (PDF)

■ AUTHOR INFORMATION

Corresponding Author

Tabrez Alam Khan − *Department of Chemistry, Jamia Millia Islamia, New Delhi 110 025, India;* orcid.org/0000-0002-2562-8836; Phone: +91 11 26985938; Email: takhan@jmi.ac.in, takhan501@yahoo.com

Authors

Suhail Ayoub Khan − *Department of Chemistry, Jamia Millia Islamia, New Delhi 110 025, India*

Mohammad Fuzail Siddiqui − *Department of Chemistry, Jamia Millia Islamia, New Delhi 110 025, India*

Complete contact information is available at: https://pubs.acs.org/10.1021/acsomega.9b03617

Notes

The authors declare no competing financial interest.

■ ACKNOWLEDGMENTS

One of the authors S.A.K. is thankful to the University Grants Commission (UGC), New Delhi, India, for financial assistance and Amity University, Noida, India, for SEM analysis.

■ REFERENCES

(1) Chen, C.; Wang, P.; Lim, T. T.; Liu, L.; Liu, S.; Xu, R. A Facile Synthesis of Monodispersed Hierarchical Layered Double Hydroxide on Silica Spheres for Efficient Removal of Pharmaceuticals from Water. *J. Mater. Chem. A* **2013**, *12*, 3877−3880.

(2) Kolpin, D. W.; Furlong, E. T.; Meyer, M. T.; Thurman, E. M.; Zaugg, S. D.; Barber, L. B.; Buxton, H. T. Pharmaceuticals, Hormones, and Other Organic Wastewater Contaminants in U.S. Streams, 1999-2000: A National Reconnaissance. *Environ. Sci. Technol.* **2002**, *36*, 1202−1211.

(3) Zhang, Y.; Habteselassie, M. Y.; Resurreccion, E. P.; Mantripragada, V.; Peng, S.; Bauer, S.; Colosi, L. M. Evaluating Removal of Steroid Estrogens by a Model Alga as a Possible Sustainability Benefit of Hypothetical Integrated Algae Cultivation and Wastewater Treatment Systems. *ACS Sustainable Chem. Eng.* **2014**, *2*, 2544−2553.

(4) Patel, M.; Kumar, R.; Kishor, K.; Mlsna, T.; Pittman, C. U.; Mohan, D. Pharmaceuticals of Emerging Concern in Aquatic Systems: Chemistry, Occurrence, Effects, and Removal Methods. *Chem. Rev.* **2019**, *119*, 3510−3673.
(5) Oberoi, A. S.; Jia, Y.; Zhang, H.; Khanal, S. K.; Lu, H. Insights into the Fate and Removal of Antibiotics in Engineered Biological Treatment Systems: A Critical Review. *Environ. Sci. Technol.* **2019**, *53*, 7234−7264.
(6) Pylypchuk, I. V.; Kessler, V. G.; Seisenbaeva, G. A. Simultaneous Removal of Acetaminophen, Diclofenac, and Cd(II) by Trametes Versicolor Laccase Immobilized on Fe_3O_4/SiO_2-DTPA Hybrid Nanocomposites. *ACS Sustainable Chem. Eng.* **2018**, *6*, 9979−9989.
(7) Badruddoza, A. Z. M.; Bhattarai, B.; Suri, R. P. S. Environmentally Friendly β-Cyclodextrin-Ionic Liquid Polyurethane-Modified Magnetic Sorbent for the Removal of PFOA, PFOS, and Cr(VI) from Water. *ACS Sustainable Chem. Eng.* **2017**, *5*, 9223−9232.
(8) Hallare, A. V.; Köhler, H. R.; Triebskorn, R. Developmental Toxicity and Stress Protein Responses in Zebrafish Embryos after Exposure to Diclofenac and Its Solvent, DMSO. *Chemosphere* **2004**, *7*, 659−666.
(9) aus der Beek, T.; Weber, F. A.; Bergmann, A.; Hickmann, S.; Ebert, I.; Hein, A.; Küster, A. Pharmaceuticals in the Environment-Global Occurrences and Perspectives. *Environ. Toxicol. Chem.* **2016**, *35*, 823−835.
(10) Evans, S. E.; Davies, P.; Lubben, A.; Kasprzyk-Hordern, B. Determination of Chiral Pharmaceuticals and Illicit Drugs in Wastewater and Sludge Using Microwave Assisted Extraction, Solid-Phase Extraction and Chiral Liquid Chromatography Coupled with Tandem Mass Spectrometry. *Anal. Chim. Acta* **2015**, *882*, 112−126.
(11) Mir-Tutusaus, J. A.; Parladé, E.; Llorca, M.; Villagrasa, M.; Barceló, D.; Rodriguez-Mozaz, S.; Martinez-Alonso, M.; Gaju, N.; Caminal, G.; Sarrà, M. Pharmaceuticals Removal and Microbial Community Assessment in a Continuous Fungal Treatment of Non-Sterile Real Hospital Wastewater after a Coagulation-Flocculation Pretreatment. *Water Res.* **2017**, *116*, 65−75.
(12) Méndez-Arriaga, F.; Torres-Palma, R. A.; Pétrier, C.; Esplugas, S.; Gimenez, J.; Pulgarin, C. Ultrasonic Treatment of Water Contaminated with Ibuprofen. *Water Res.* **2008**, *42*, 4243−4248.
(13) Russo, D.; Siciliano, A.; Guida, M.; Galdiero, E.; Amoresano, A.; Andreozzi, R.; Reis, N. M.; Li Puma, G.; Marotta, R. Photodegradation and Ecotoxicology of Acyclovir in Water under UV254 and UV 254/H_2O_2 processes. *Water Res.* **2017**, *42*, 4243−4248.
(14) Liu, X.; Yang, D.; Zhou, Y.; Zhang, J.; Luo, L.; Meng, S.; Chen, S.; Tan, M.; Li, Z.; Tang, L. Electrocatalytic Properties of N-Doped Graphite Felt in Electro-Fenton Process and Degradation Mechanism of Levofloxacin. *Chemosphere* **2017**, *182*, 306−315.
(15) Isarain-Chávez, E.; Rodríguez, R. M.; Cabot, P. L.; Centellas, F.; Arias, C.; Garrido, J. A.; Brillas, E. Degradation of Pharmaceutical Beta-Blockers by Electrochemical Advanced Oxidation Processes Using a Flow Plant with a Solar Compound Parabolic Collector. *Water Res.* **2011**, *14*, 4119−4130.
(16) Mudassir, M. A.; Hussain, S. Z.; Jilani, A.; Zhang, H.; Ansari, T. M.; Hussain, I. Magnetic Hierarchically Macroporous Emulsion-Templated Poly(Acrylic Acid)−Iron Oxide Nanocomposite Beads for Water Remediation. *Langmuir* **2019**, *35*, 8996−9003.
(17) Khan, E. A.; Shahjahan & Khan, T. A. Adsorption of Methyl Red on Activated Carbon derived from Custard Apple (*Annona squamosa*) Fruit Shell: Equilibrium Isotherm and Kinetic Studies. *J. Mol. Liq.* **2018**, *107*, 70−77.
(18) Limousy, L.; Ghouma, I.; Ouederni, A.; Jeguirim, M. Amoxicillin Removal from Aqueous Solution Using Activated Carbon Prepared by Chemical Activation of Olive Stone. *Environ. Sci. Pollut. Res.* **2017**, *107*, 70−77.
(19) Pouretedal, H. R.; Sadegh, N. Effective Removal of Amoxicillin, Cephalexin, Tetracycline and Penicillin G from Aqueous Solutions Using Activated Carbon Nanoparticles Prepared from Vine Wood. *J. Water Process Eng.* **2014**, *1*, 64−73.
(20) Pezoti, O.; Cazetta, A. L.; Bedin, K. C.; Souza, L. S.; Martins, A. C.; Silva, T. L.; Santos Júnior, O. O.; Visentainer, J. V.; Almeida, V. C. NaOH-Activated Carbon of High Surface Area Produced from Guava Seeds as a High-Efficiency Adsorbent for Amoxicillin Removal: Kinetic, Isotherm and Thermodynamic Studies. *Chem. Eng. J.* **2016**, *288*, 778−788.
(21) Viotti, P. V.; Moreira, W. M.; dos Santos, O. A. A.; Bergamasco, R.; Vieira, A. M. S.; Vieira, M. F. Diclofenac Removal from Water by Adsorption on *Moringa oleifera* Pods and Activated Carbon: Mechanism, Kinetic and Equilibrium Study. *J. Clean. Prod.* **2019**, *219*, 809−817.
(22) Naghipour, D.; Hoseinzadeh, L.; Taghavi, K.; Jaafari, J. Characterization, Kinetic, Thermodynamic and Isotherm Data for Diclofenac Removal from Aqueous Solution by Activated Carbon Derived from Pine Tree. *Data Br.* **2018**, *18*, 1082−1087.
(23) Liu, H.; Hu, Z.; Liu, H.; Xie, H.; Lu, S.; Wang, Q.; Zhang, J. Adsorption of Amoxicillin by Mn-Impregnated Activated Carbons: Performance and Mechanisms. *RSC Adv.* **2016**, *6*, 11454−11460.
(24) Crisafully, R.; Milhome, M. A. L.; Cavalcante, R. M.; Silveira, E. R.; De Keukeleire, D.; Nascimento, R. F. Removal of Some Polycyclic Aromatic Hydrocarbons from Petrochemical Wastewater Using Low-Cost Adsorbents of Natural Origin. *Bioresour. Technol.* **2008**, *10*, 4515−4519.
(25) Peng, N.; Hu, D.; Zeng, J.; Li, Y.; Liang, L.; Chang, C. Superabsorbent Cellulose-Clay Nanocomposite Hydrogels for Highly Efficient Removal of Dye in Water. *ACS Sustainable Chem. Eng.* **2016**, *4*, 7217−7224.
(26) Jana, S.; Ray, J.; Mondal, B.; Tripathy, T. Efficient and Selective Removal of Cationic Organic Dyes from Their Aqueous Solutions by a Nanocomposite Hydrogel, Katira Gum-Cl-Poly(Acrylic Acid-Co-N, N-Dimethylacrylamide)@bentonite. *Appl. Clay Sci.* **2019**, *173*, 46−64.
(27) Bhattacharyya, R.; Ray, S. K. Removal of Congo Red and Methyl Violet from Water Using Nano Clay Filled Composite Hydrogels of Poly Acrylic Acid and Polyethylene Glycol. *Chem. Eng. J.* **2015**, *260*, 269−283.
(28) Wang, W.; Zhao, Y.; Yi, H.; Chen, T.; Kang, S.; Zhang, T.; Rao, F.; Song, S. Pb(II) Removal from Water Using Porous Hydrogel of Chitosan-2D Montmorillonite. *Int. J. Biol. Macromol.* **2019**, *128*, 85−93.
(29) Vieira, R. M.; Vilela, P. B.; Becegato, V. A.; Paulino, A. T. Chitosan-Based Hydrogel and Chitosan/Acid-Activated Montmorillonite Composite Hydrogel for the Adsorption and Removal of Pb^{+2} and Ni^{+2} Ions Accommodated in Aqueous Solutions. *J. Environ. Chem. Eng.* **2018**, *6*, 2713−2723.
(30) Sun, X. F.; Hao, Y.; Cao, Y.; Zeng, Q. Superadsorbent Hydrogel Based on Lignin and Montmorillonite for Cu(II) Ions Removal From Aqueous Solution. *Int. J. Biol. Macromol.* **2019**, *127*, 511−519.
(31) Khan, S. A.; Siddiqui, M. F.; Khan, T. A. Ultrasonic-Assisted Synthesis of Polyacrylamide / Bentonite Hydrogel Nanocomposite for the Sequestration of Lead and Cadmium from Aqueous Phase: Equilibrium, Kinetics and Thermodynamic Studies. *Ultrason. Sonochem.* **2020**, *60*, No. 104761.
(32) Qader, H. A.; Fakhre, N. A. Spectrophotometric Determination of Amoxicillin Trihydrate in Pure and Pharmaceutical Dosage Forms. *Ibn AL-Haitham J. Pure Appl. Sci.* **2017**, *28*, 142−153.
(33) Agrawal, Y. K.; Shivramchandra, K. Spectrophotometric Determination of Diclofenac Sodium in Tablets. *J. Pharmaceut. Biomed. Anal.* **1991**, *9*, 97−100.
(34) Zhi, Y.; Li, Y.; Zhang, Q.; Wang, H. ZnO Nanoparticles Immobilized on Flaky Layered Double Hydroxides as Photocatalysts with Enhanced Adsorptivity for Removal of Acid Red G. *Langmuir* **2010**, *26*, 15546−15553.
(35) Bartolozzi, A.; Bertani, R.; Burigo, E.; Fabrizi, A.; Panozzo, F.; Quaresimin, M.; Simionato, F.; Sgarbossa, P.; Tamburini, S.; Zappalorto, M.; Federico, Z. Multifunctional Cu^{2+} -Montmorillonite/Epoxy Resin Nanocomposites with Antibacterial Activity. *J. Appl. Polym. Sci.* **2017**, *134*, 1−11.

https://dx.doi.org/10.1021/acsomega.9b03617
ACS Omega 2020, 5, 2843−2855

(36) Liao, L.; Lv, G.; Cai, D.; Wu, L. The Sequential Intercalation of Three Types of Surfactants into Sodium Montmorillonite. *Appl. Clay Sci.* **2016**, *119*, 82−86.
(37) Yan, H.; Chen, X.; Feng, Y.; Xiang, F.; Li, J.; Shi, Z.; Wang, X.; Lin, Q. Modification of Montmorillonite by Ball-Milling Method for Immobilization and Delivery of Acetamiprid Based on Alginate/Exfoliated Montmorillonite Nanocomposite. *Polym. Bull.* **2016**, *73*, 1185−1206.
(38) Moslemizadeh, A.; Khezerloo-ye Aghdam, S.; Shahbazi, K.; Khezerloo-ye Aghdam, H.; Alboghobeish, F. Assessment of Swelling Inhibitive Effect of CTAB Adsorption on Montmorillonite in Aqueous Phase. *Appl. Clay Sci.* **2016**, *127*, 111−122.
(39) Maity, J.; Ray, S. K. Enhanced Adsorption of Methyl Violet and Congo Red by Using Semi and Full IPN of Polymethacrylic Acid and Chitosan. *Carbohydr. Polym.* **2014**, *104*, 8−16.
(40) Zha, S. x.; Zhou, Y.; Jin, X.; Chen, Z. The Removal of Amoxicillin from Wastewater Using Organobentonite. *J. Environ. Manage.* **2013**, *129*, 569−576.
(41) Kenawy, E. R.; Ghfar, A. A.; Wabaidur, S. M.; Khan, M. A.; Siddiqui, M. R.; Alothman, Z. A.; Alqadami, A. A.; Hamid, M. Cetyltrimethylammonium Bromide Intercalated and Branched Polyhydroxystyrene Functionalized Montmorillonite Clay to Sequester Cationic Dyes. *J. Environ. Manage.* **2018**, *219*, 285−293.
(42) Natkański, P.; Kuśtrowski, P.; Białas, A.; Piwowarska, Z.; Michalik, M. Controlled Swelling and Adsorption Properties of Polyacrylate/Montmorillonite Composites. *Mater. Chem. Phys.* **2012**, *136*, 1109−1115.
(43) Yan, S.; Cai, Y.; Li, H.; Song, S.; Xia, L. Enhancement of Cadmium Adsorption by EPS-Montmorillonite Composites. *Environ. Pollut.* **2019**, *252*, 1509−1518.
(44) Afkhami, A.; Saber-Tehrani, M.; Bagheri, H. Modified Maghemite Nanoparticles as an Efficient Adsorbent for Removing Some Cationic Dyes from Aqueous Solution. *Desalination* **2010**, *3*, 240−248.
(45) Hu, D.; Wang, L. Adsorption of Amoxicillin onto Quaternized Cellulose from Flax Noil: Kinetic, Equilibrium and Thermodynamic Study. *J. Taiwan Inst. Chem. Eng.* **2016**, *64*, 227−234.
(46) Zhu, L.; Chen, B.; Shen, X. Sorption of Phenol, p-Nitrophenol, and Aniline to Dual-Cation Organobentonites from Water. *Environ. Sci. Technol.* **2000**, *3*, 468−475.
(47) Kerkez-Kuyumcu, Ö.; Bayazit, Ş. S.; Salam, M. A. Antibiotic Amoxicillin Removal from Aqueous Solution Using Magnetically Modified Graphene Nanoplatelets. *J. Ind. Eng. Chem.* **2016**, *36*, 198−205.
(48) Bhadra, B. N.; Seo, P. W.; Jhung, S. H. Adsorption of Diclofenac Sodium from Water Using Oxidized Activated Carbon. *Chem. Eng. J.* **2016**, *301*, 27−34.
(49) Fang, R.; He, W.; Xue, H.; Chen, W. Synthesis and Characterization of a High-Capacity Cationic Hydrogel Adsorbent and Its Application in the Removal of Acid Black 1 from Aqueous Solution. *React. Funct. Polym.* **2016**, *102*, 1−10.
(50) Siddiqui, M. F.; Khan, E. A.; Khan, T. A. Synthesis of MoO_3/Polypyrrole Nanocomposite and Its Adsorptive Properties toward Cadmium(II) and Nile Blue from Aqueous Solution: Equilibrium Isotherm and Kinetics Modeling. *Environ. Prog. Sustainable Energy* **2019**, No. e13249.
(51) Weng, X.; Lin, S.; Zhong, Y.; Chen, Z. Chitosan Stabilized Bimetallic Fe/Ni Nanoparticles Used to Remove Mixed Contaminants-Amoxicillin and Cd(II) from Aqueous Solutions. *Chem. Eng. J.* **2013**, *229*, 27−34.
(52) Anggraini, M.; Kurniawan, A.; Ong, L. K.; Martin, M. A.; Liu, J. C.; Soetaredjo, F. E.; Indraswati, N.; Ismadji, S. Antibiotic Detoxification from Synthetic and Real Effluents Using a Novel MTAB Surfactant-Montmorillonite (Organoclay) Sorbent. *RSC Adv.* **2014**, *31*, 16298−16311.
(53) Li, H.; Hu, J.; Cao, Y.; Li, X.; Wang, X. Development and Assessment of a Functional Activated Fore-Modified Bio-Hydrochar for Amoxicillin Removal. *Bioresour. Technol.* **2017**, *246*, 168−175.
(54) Gil, A.; Santamaría, L.; Korili, S. A. Removal of Caffeine and Diclofenac from Aqueous Solution by Adsorption on Multiwalled Carbon Nanotubes. *Colloids Interface Sci. Commun.* **2018**, *22*, 25−28.
(55) Sekulic, M. T.; Boskovic, N.; Slavkovic, A.; Garunovic, J.; Kolakovic, S.; Pap, S. Surface Functionalised Adsorbent for Emerging Pharmaceutical Removal: Adsorption Performance and Mechanisms. *Process Saf. Environ. Prot.* **2019**, *125*, 50−63.
(56) Lin, K. Y.; Yang, H.; Lee, W. D. Enhanced Removal of Diclofenac from Water Using a Zeolitic Imidazole Framework Functionalized with Cetyltrimethylammonium Bromide (CTAB). *RSC Adv.* **2015**, *99*, 81330−81340.
(57) Sathishkumar, P.; Arulkumar, M.; Ashokkumar, V.; Mohd Yusoff, A. R.; Murugesan, K.; Palvannan, T.; Salam, Z.; Ani, F. N.; Hadibarata, T. Modified Phyto-Waste *Terminalia catappa* Fruit Shells: A Reusable Adsorbent for the Removal of Micropollutant Diclofenac. *RSC Adv.* **2015**, *39*, 30950−30962.
(58) Vedenyapina, M. D.; Stopp, P.; Weichgrebe, D.; Vedenyapin, A. A. Adsorption of Diclofenac Sodium from Aqueous Solutions on Activated Carbon. *Solid Fuel Chem.* **2016**, *1*, 46−55.
(59) Tomul, F.; Arslan, Y.; Başoğlu, F. T.; Babuçcuoğlu, Y.; Tran, H. N. Efficient Removal of Anti-Inflammatory from Solution by Fe-Containing Activated Carbon: Adsorption Kinetics, Isotherms, and Thermodynamics. *J. Environ. Manage.* **2019**, *238*, 296−306.
(60) Freundlich, H. M. F. Over the Adsorption in Solution. *J. Phys. Chem. A* **1906**, *57*, 385−470.
(61) Dubinin, M. M.; Radushkevich, L. V. The Equation of the Characteristic Curve of Activated Charcoal. *Proc. Acad. Sci. Phys. Chem. Sect.* **1947**, *1*, 875.
(62) Hussain, D.; Siddiqui, M. F.; Khan, T. A. Preparation of $NiFe_2O_4$/polythiophene nanocomposite and its enhanced adsorptive uptake of Janus green B and Fuchsin basic from aqueous solution: Isotherm and kinetics studies. *Environ. Prog. Sustainable Energy* **2019**, No. e13371.
(63) Hu, X. S.; Liang, R.; Sun, G. Super-Adsorbent Hydrogel for Removal of Methylene Blue Dye from Aqueous Solution. *J. Mater. Chem. A* **2018**, *36*, 17612−17624.
(64) Weber, W. J.; Morris, J. C. Kinetics of Adsorption on Carbon From Solution. *J. Sanit. Eng. Div.* **1963**, *2*, 31−60.
(65) Zhao, Y.; Li, W.; Liu, Z.; Liu, J.; Zhu, L.; Liu, X.; Huang, K. Renewable Tb/Eu-Loaded Garlic Peels for Enhanced Adsorption of Enrofloxacin: Kinetics, Isotherms, Thermodynamics, and Mechanism. *ACS Sustainable Chem. Eng.* **2018**, *6*, 15264−15272.
(66) Zhao, Q.; Burns, S. E. Modeling Sorption and Diffusion of Organic Sorbate in Hexadecyltrimethylammonium-Modified Clay Nanopores - A Molecular Dynamics Simulation Study. *Environ. Sci. Technol.* **2013**, *6*, 2769−2776.
(67) Boyd, G. E.; Schubert, J.; Adamson, A. W. The Exchange Adsorption of Ions from Aqueous Solutions by Organic Zeolites. Ion-Exchange Equilibria. *J. Am. Chem. Soc.* **1947**, *11*, 2836−2848.
(68) Chowdhury, A.; Khan, A. A.; Kumari, S.; Hussain, S. Superadsorbent Ni-Co-S/SDS Nanocomposites for Ultrahigh Removal of Cationic, Anionic Organic Dyes and Toxic Metal Ions: Kinetics, Isotherm and Adsorption Mechanism. *ACS Sustainable Chem. Eng.* **2019**, *7*, 4165−4176.
(69) Yadav, M.; Das, M.; Savani, C.; Thakore, S.; Jadeja, R. Maleic Anhydride Cross-Linked β-Cyclodextrin-Conjugated Magnetic Nanoadsorbent: An Ecofriendly Approach for Simultaneous Adsorption of Hydrophilic and Hydrophobic Dyes. *ACS Omega* **2019**, *4*, 11993−12003.
(70) Ye, Y.; Hu, Y.; Hussain, Z.; Li, X.; Li, D.; Kang, J. Simultaneous Adsorptive Removal of Fluoride and Phosphate by Magnesia-Pullulan Composite from Aqueous Solution. *RSC Adv.* **2016**, *6*, 35966−35976.

https://dx.doi.org/10.1021/acsomega.9b03617
ACS Omega 2020, 5, 2843−2855